Journal of Computational Physics **183,** 438–469 (2002)
doi:10.1006/jcph.2002.7201

A New Compact Spectral Scheme for Turbulence Simulations

Changhoon Lee and Youngchwa Seo

School of Mechanical Engineering, Yonsei University, Seoul, Korea
E-mail: clee@yonsei.ac.kr

Received April 25, 2001; revised May 1, 2002

We propose a new kind of compact difference scheme for the computation of the first and second derivatives in the simulation of high-Reynolds number turbulent flows. The scheme combines and truncates the pseudospectral representation of derivative for convergence acceleration. Comparison of the wave resolution property with available optimized compact schemes minimizing the prescribed wave resolution error reveals our scheme's superiority for the same size of stencils without introducing optimization parameters. An accompanying boundary scheme is also proposed with the stability analysis. The proposed scheme is tested for the evaluation of derivatives of a function that decays very slowly in the wavenumber space, and for the simulation of three-dimensional isotropic turbulence.

Key Words: compact spectral scheme; turbulence simulation; wave resolution.

1. INTRODUCTION

Direct numerical simulation (DNS) of high-Reynolds number turbulent flows requires a derivative scheme that has a good wave resolution property. The energy spectrum in typical three-dimensional turbulence decays very slowly in the inertial subrange, i.e., $E(\kappa) \sim \kappa^{-5/3}$, where κ is the wavenumber. This implies that the Fourier component of velocity, $|\hat{u}_\kappa| \sim \kappa^{-1/3}$, and the vorticity component increases with the wavenumber, i.e., $|\hat{\omega}_\kappa| \sim \kappa^{2/3}$, in the inertial range. Most DNS studies have been carried out with marginal grid resolution due to a strict requirement of computation time. For example, the grid size is chosen to be several times larger than the Kolmogorov length scale. In large eddy simulations (LES), the filtering places the maximum resolved wavenumber in the middle of the inertial range. Therefore, the energy spectrum is very flat in the resolved wavenumber range. This requires a derivative scheme to possess a good wave resolution capability especially in the wavenumber range near the maximum resolved wavenumber as it is essential to correctly simulate the small-scale dynamics in either DNS or LES. Although in real applications, the aliasing error resulting from the quadratic nonlinear terms in the integration of

0021-9991/02 $35.00

the Navier–Stokes equations contaminates small-scale components, the use of high-order differencing schemes is strongly encouraged [1, 2].

For the perfect resolution of small-scale motions, a spectral scheme is an obvious choice, but the scheme is restricted to a case with a simple domain. A compact finite difference scheme was proposed by Lele [3] to obtain a good wave resolution property by combining derivatives in the neighborhood in the finite difference context. This idea of combining was extended by Chu and Fan [4] and Mahesh [5] in their combined compact schemes and coupled-derivative schemes, respectively. Their idea is basically to produce a high-order scheme by combining and solving the first and second derivatives together. The high-order truncation error of their schemes, however, is effective in the low wavenumber range since these schemes were developed through an investigation of the truncation error.

On the other hand, a variety of optimized schemes were proposed for application to computations of aeroacoustic or electromagnetic wave propagation. These schemes optimize the coefficients of the scheme to improve wave resolving performance at the expense of truncation errors. Several schemes were developed through minimization procedures of the prescribed wave resolution errors for explicit centered difference schemes (see [6–8]) and for the upwind schemes (see [9–12]). The same idea was further facilitated to derive compact optimized schemes by minimizing a measure of wave resolving capability over a high-dimensional optimization parameter space (see [13–15]). This approach produced schemes with the best wave resolution property so far.

Another kind of attempt was made to derive schemes from truncated pseudospectral approximation. Boyd [16, 17] investigated the possibility of deriving a sparse but spectrally accurate differentiation scheme using the cardinal sinc function approximation. Poor convergence of the truncated sinc function approximation was improved by the Euler-sum acceleration. The wave resolution performance, however, was not good compared to explicit or compact high-order finite difference schemes. Viewing the finite difference approximation as an accelerated sinc approximation with particular weights, Boyd [18] proposed a spectrally weighted least squares difference scheme employing the hyperbolic secant function, resulting in a slightly better performance than that of finite difference schemes.

In the early stage of our study, we started with a truncated pseudospectral approximation in the infinite domain which is identical to the sinc function approximation of Boyd. We noted that the coefficients of the sinc function difference decay with alternating signs as was done by Boyd [16]. Instead of using the Euler-sum acceleration, however, we combined the expressions of derivatives in the neighborhood to cancel out the coefficients, thereby accelerating the convergence of the approximation. Although the resulting scheme has a form similar to that of the compact finite difference scheme, the path of derivation is totally different. Our goal in this study is to derive a very efficient scheme by using a unique approach and compare the performance of the proposed scheme with other known schemes such as the compact finite difference scheme (CS) and optimized schemes of various sorts. Our scheme will be referred to as the compact spectral scheme (CSS).

The paper is organized as follows. In Section 2, the derivation of our scheme is presented. Comparisons with other known optimized schemes are made in Section 3. Accompanying boundary schemes are explained in Section 4 followed by Section 5 in which the scheme is tested for the simulation of three-dimensional isotropic homogeneous turbulence. Section 6 concludes the paper.

2. COMPACT SPECTRAL SCHEME

2.1. Pseudospectral Approximation

Consider a periodic function $u(x)$ having the period L. The discretized representation is $u_j(=u(j\Delta x))$, $j=1,\ldots,N$, where $\Delta x = L/N$. A discrete spectral representation for the first derivative can be expressed in closed form as [20]

$$u'_j = \sum_{k=1}^{N} D_{jk} u_k, \quad \text{for } j=1,\ldots,N \tag{1}$$

with

$$D_{jk} = 0 \qquad \text{if } j=k \tag{2}$$

$$= \frac{1}{2}(-1)^{j+k} \cot\left(\frac{(j-k)\Delta x}{2}\right) \quad \text{if } j \neq k. \tag{3}$$

If $u_j = \exp(ij\kappa\Delta x)$ with wavenumber κ, we can define the modified wavenumber, $\kappa'(\kappa_k) \equiv u'_j/(iu_j)$. The modified wavenumber for this spectral scheme then becomes exactly equal to κ at discrete points, κ_k, meaning perfect wave resolution in a discrete manner. The matrix D_{jk}, however, is a full matrix, requiring N^2 operations to invert. The fast Fourier transform can be used to reduce the number of operations to $\sim N \log N$. We observe here that $|D_{jk}|$ decays with $|j-k|$ until $|j-k| = N/2-1$ and then increases again in a periodic manner. To apply the scheme to a nonperiodic function, we let L and N go to infinity keeping $\Delta x(=L/N)$ constant. Then for $|j-k| \ll N$, the off-diagonal element of D_{jk} becomes

$$D_{jk} \simeq \frac{(-1)^{j+k}}{(j-k)\Delta x}. \tag{4}$$

Note that the matrix element is a skew-symmetric function of $j-k$ only and the sign of the element alternates with $j-k$ and that the magnitude of the element decays with $|j-k|$. Therefore it may be possible to truncate the series so that the resulting representation for the first derivative can be written as

$$u'_j = \sum_{l=-M}^{M} d_l u_{j+l} \tag{5}$$

with

$$d_l = 0 \qquad \text{if } l=0 \tag{6}$$

$$= \frac{(-1)^{l+1}}{l\Delta x} \quad \text{if } l \neq 0, \tag{7}$$

where M denotes the maximum number of terms retained in each direction on the right-hand side of the scheme. However, this expression is not useful since the coefficient decays very slowly, $\sim 1/l$, and thus the convergence is poor. We will discuss how to improve the convergence in the following section.

For the second derivative, a similar representation can be obtained if using the convolution of the coefficient for the first derivative calculation.

$$d_l^{(2)} = \sum_{k=-\infty}^{\infty} d_{l-k}\, d_k. \tag{8}$$

Using $\sum_{k=1}^{\infty} 1/k^2 = \pi^2/6$, we obtain the following expression of the coefficient for the second derivative.

$$d_l^{(2)} = -\frac{\pi^2}{3\Delta x^2} \quad \text{if } l = 0 \tag{9}$$

$$= \frac{2(-1)^{l+1}}{l^2 \Delta x^2} \quad \text{if } l \neq 0. \tag{10}$$

Although the coefficient for the second derivative decays a little faster ($\sim 1/l^2$) than that for the first derivative, the scheme is still not good enough to produce a reliable second derivative. This derivation is easily generalized to the high-order derivatives and the coefficients are presented in Table I. The coefficients for the odd-numbered derivatives decay as $\sim 1/l$ while those for the even-numbered derivatives decay quadratically, $\sim 1/l^2$, the signs for both cases alternating. This can be understood as follows. By the convolution theorem, the Fourier transform of the derivative coefficient, $d_l^{(n)}$, alone will approximate a periodic function $\hat{d}_\kappa^{(n)} = (i\kappa)^n$ with a period $2\kappa_{max}$ in the region $-\kappa_{max} \leq \kappa \leq \kappa_{max}$ with $\kappa_{max} = \pi/\Delta x$ for each n. For an odd n, this function is not continuous at $\kappa = \pm\kappa_{max}$; hence the inverse Fourier coefficient, d_l, decays as $\sim 1/l$. For an even n, however, the first derivative of $\hat{d}_\kappa^{(n)}$ with respect to κ is not continuous at $\kappa = \pm\kappa_{max}$. Therefore, d_l decays as $\sim 1/l^2$.

The coefficients in Table I are not useful unless a great number of terms are included to calculate derivatives of each order. These coefficients are exactly the same as the derivative coefficients approximating a function in the infinite domain using the cardinal sinc function [19]. Boyd [16, 17] employed the Euler-sum acceleration to improve the convergence of the series representation for the first and second derivatives since the sign of the series alternates. We also investigated this issue by using several acceleration methods including the Euler-sum acceleration and Chebyshev weights [21] and found that the resulting schemes

TABLE I

Expressions for $d_l^{(n)}$

n	$d_0^{(n)} \Delta x^n$	$d_l^{(n)} \Delta x^n$ $(l \neq 0)$
1	0	$\frac{(-1)^{l+1}}{l}$
2	$-\frac{\pi^2}{3}$	$\frac{2(-1)^{l+1}}{l^2}$
3	0	$\frac{\pi^2(-1)^l}{l}\left(1 - \frac{6}{\pi^2 l^2}\right)$
4	$\frac{\pi^4}{5}$	$\frac{4\pi^2(-1)^l}{l^2}\left(1 - \frac{6}{\pi^2 l^2}\right)$
5	0	$\frac{\pi^4(-1)^{l+1}}{l}\left(1 - \frac{20}{\pi^2 l^2} + \frac{120}{\pi^4 l^4}\right)$
6	$-\frac{\pi^6}{7}$	$\frac{6\pi^4(-1)^{l+1}}{l^2}\left(1 - \frac{20}{\pi^2 l^2} + \frac{120}{\pi^4 l^4}\right)$

still do not have a good wave resolution property and that many terms should be included to produce a reasonable approximation.

2.2. Convergence Acceleration

The goal of this paper is to develop a scheme that requires only a few terms to calculate derivatives and still has a good wave resolution property. The pseudospectral representation discussed in the previous section shows a very poor convergence property even when an acceleration method for an alternating series is used. To improve the convergence, we take advantage of the sign-alternating property of the coefficients by combining derivatives in the neighborhood. First, we express the derivative scheme using the symmetry of the coefficient as follows.

$$u_j^{(n)} = \sum_{l=1}^{\infty} d_l^{(n)}(u_{j+l} - u_{j-l}) \qquad \text{for } n = \text{odd} \tag{11}$$

$$u_j^{(n)} = d_0^{(n)} u_j + \sum_{l=1}^{\infty} d_l^{(n)}(u_{j+l} + u_{j-l}) \quad \text{for } n = \text{even} \tag{12}$$

with $d_l^{(n)}$ listed in Table I. We then consider the following combination for the first and second derivatives.

$$\beta u'_{j-2} + \alpha u'_{j-1} + u'_j + \alpha u'_{j+1} + \beta u'_{j+2} = \sum_{l=1}^{M} \mathcal{D}_l^{(1)}(\alpha, \beta)(u_{j+l} - u_{j-l}), \tag{13}$$

$$\beta u''_{j-2} + \alpha u''_{j-1} + u''_j + \alpha u''_{j+1} + \beta u''_{j+2} = \mathcal{D}_0^{(2)}(\alpha, \beta) u_j + \sum_{l=1}^{M} \mathcal{D}_l^{(2)}(\alpha, \beta)(u_{j+l} + u_{j-l}), \tag{14}$$

where $\mathcal{D}_l^{(n)}(\alpha, \beta)$ is a function of α and β only and is presented in Tables II and III for the first and second derivatives, respectively. Here, M is the number of terms retained in each direction after combining. It should be noted that the series is truncated after the expressions for derivatives in the neighborhood are combined. This combination is expected to reduce the error by canceling out the terms in derivative expression since the sign of $d_l^{(n)}$ alternates with l as shown in Table I. Then we may expect that $\mathcal{D}_l^{(n)}$ decays faster with l. This scheme should be distinguished from the compact finite difference scheme or other

TABLE II
$\mathcal{D}_l^{(1)}$

l	$\mathcal{D}_l^{(1)}(\alpha, \beta)\Delta x$
1	$1 - \frac{1}{2}\alpha - \frac{2}{3}\beta$
2	$-\frac{1}{2} + \frac{4}{3}\alpha - \frac{1}{4}\beta$
$l > 2$	$(-1)^{l+1} \frac{(1 - 2\alpha + 2\beta)l^4 + (-5 + 8\alpha - 2\beta)l^2 + 4}{l(l^2 - 1)(l^2 - 4)}$

TABLE III
$\mathcal{D}_l^{(2)}$

l	$\mathcal{D}_l^{(2)}(\alpha,\beta)\Delta x^2$
0	$-2\sum_{l=1}^{M}\mathcal{D}_l^{(2)}(\alpha,\beta)\Delta x^2$
1	$2-\left(\frac{1}{2}+\frac{\pi^2}{3}\right)\alpha+\frac{20}{9}\beta$
2	$-\frac{1}{2}+\frac{20}{9}\alpha-\left(\frac{1}{8}+\frac{\pi^2}{3}\right)\beta$
$l>2$	$2(-1)^{l+1}\frac{(1-2\alpha+2\beta)l^8+(-10+14\alpha+4\beta)l^6+(33-16\alpha-14\beta)l^4+(-40-32\alpha+8\beta)l^2+16}{l^2(l^2-1)^2(l^2-4)^2}$

optimized schemes in that our scheme maintains the pseudospectral representation on the right-hand side while only two degrees of freedom are allowed on the left-hand side. We will consider the $\beta=0$ case (one degree of freedom) and nonzero β case (two degrees of freedom) together in the following derivation.

The expression for $\mathcal{D}_l^{(n)}$ is independent of the degree of truncation, M, except for $\mathcal{D}_0^{(2)}$. The value of $\mathcal{D}_0^{(2)}$ is modified as shown in the table such that the scheme correctly produces the second derivative of $u(x)=$ constant. This does not spoil the accuracy of the scheme when applied to a general case since this shift-invariance property can always shift the function such that $u_j=0$ in the calculation of the second derivative at $x=j\Delta x$; then $\mathcal{D}_0^{(2)}$ does not affect the computation.

A selection of α and β completely determines $\mathcal{D}_l^{(n)}(\alpha,\beta)$. From the general expression of $\mathcal{D}_l^{(n)}(\alpha,\beta)$ for $l>2$ in Tables II and III, it might be conjectured that a selection of α and β so that the coefficients of the highest two terms in l in the numerator vanish would result in $\mathcal{D}_l^{(n)}(\alpha,\beta)$ decaying faster, meaning better convergence. For example, for the first derivative, α and β can be chosen to satisfy $1-2\alpha+2\beta=0$ and $-5+8\alpha-2\beta=0$ simultaneously, yielding $\alpha=1/2$ when β is set to zero and $\alpha=1/3$ and $\beta=1/6$ for the nonzero β case. Then $\mathcal{D}_l^{(1)}(\alpha,\beta)$ decays as $\sim 1/l^3$ when $\alpha=1/2$ and $\beta=0$ and as $\sim 1/l^5$ when $\alpha=1/3$ and $\beta=1/6$. In fact we cannot choose α and β in such a way since this selection would cause the scheme to be singular at the maximum wavenumber as will be shown below.

To investigate this issue further and determine α and β, we examine the modified wavenumber. If $u_j=e^{ij\kappa\Delta x}$ is substituted into Eqs. (13) and (14), we can define the modified wavenumber as $\kappa'(\kappa)\equiv u_j'/(iu_j)$ and $\kappa''(\kappa)\equiv -u_j''/u_j$ for the first and second derivatives, respectively. Now, $\kappa'(\kappa)$ and $\kappa''(\kappa)$ are functions of the continuous variable κ since the domain is infinite. However, κ is bounded by $\kappa_{max}(=\pi/\Delta x)$. Exact wave resolution means $\kappa'=\kappa$ or $\kappa''=\kappa^2$. The modified wavenumbers normalized by κ_{max} and κ_{max}^2, respectively for Eqs. (13) and (14) become

$$\frac{\kappa'}{\kappa_{max}}\left(\frac{\kappa}{\kappa_{max}};\alpha,\beta\right)=\frac{2\Delta x\sum_{l=1}^{M}\mathcal{D}_l^{(1)}(\alpha,\beta)\sin\left(\frac{l\pi\kappa}{\kappa_{max}}\right)}{\pi\left(1+2\alpha\cos\left(\frac{\pi\kappa}{\kappa_{max}}\right)+2\beta\cos\left(\frac{2\pi\kappa}{\kappa_{max}}\right)\right)},\tag{15}$$

$$\frac{\kappa''}{\kappa_{max}^2}\left(\frac{\kappa}{\kappa_{max}};\alpha,\beta\right)=\frac{-2\Delta x^2\sum_{l=1}^{M}\mathcal{D}_l^{(2)}(\alpha,\beta)\left(1-\cos\left(\frac{l\pi\kappa}{\kappa_{max}}\right)\right)}{\pi^2\left(1+2\alpha\cos\left(\frac{\pi\kappa}{\kappa_{max}}\right)+2\beta\cos\left(\frac{2\pi\kappa}{\kappa_{max}}\right)\right)}.\tag{16}$$

The first necessary condition for these schemes to be useful is that the denominator should

not vanish in the range $0 \le \kappa \le \kappa_{max}$. This leads to

$$1 - 2\alpha + 2\beta > 0, \tag{17}$$

meaning that the coefficient of the highest term in the numerator of $\mathcal{D}_l^{(1)}(\alpha, \beta)$ and $\mathcal{D}_l^{(2)}(\alpha, \beta)$ for $l > 2$ cannot vanish.

For a unique determination of α and β, we examine the formal accuracy of the scheme. Because of the symmetry of the coefficient and the shift-invariance property, the first derivative of an even function is exactly zero and the second derivative of an odd function is exactly zero. The first two functions for which the scheme cannot exactly yield the first derivative are linear and cubic functions. The condition that the scheme accurately produce the first derivative of a linear or cubic function can be realized in several ways. We choose the following approach. We select α and β such that the normalized modified wavenumber best approximate the exact wavenumber near $\kappa = 0$. This immediately yields the conditions

$$\left.\frac{d(\kappa'/\kappa_{max})}{d(\kappa/\kappa_{max})}\right|_{\kappa=0} = 1, \tag{18}$$

$$\left.\frac{d^3(\kappa'/\kappa_{max})}{d(\kappa/\kappa_{max})^3}\right|_{\kappa=0} = 0 \tag{19}$$

from which α and β are uniquely determined for the first derivative scheme. The similar conditions for the second derivative are

$$\left.\frac{d^2(\kappa''/\kappa_{max})}{d(\kappa/\kappa_{max})^2}\right|_{\kappa=0} = 2, \tag{20}$$

$$\left.\frac{d^4(\kappa'/\kappa_{max})}{d(\kappa/\kappa_{max})^4}\right|_{\kappa=0} = 0. \tag{21}$$

This guarantees the fourth-order accuracy for the first and second derivative scheme. The choice of $\beta = 0$ reduces the scheme to the second-order scheme. The corresponding α when $\beta = 0$, or α and β for several M's are listed in Tables IV and V. When $\beta = 0$, the scheme

TABLE IV

α and β for the First Derivative Scheme

M	$(\alpha, 0)$	(α, β)
1	$\left(\frac{1}{3}, 0\right)$	$\left(\frac{28}{79}, -\frac{3}{158}\right)$
2	$\left(\frac{3}{7}, 0\right)$	$\left(\frac{10}{19}, \frac{1}{19}\right)$
3	$\left(\frac{6}{13}, 0\right)$	$\left(\frac{32}{55}, \frac{1}{11}\right)$
4	$\left(\frac{10}{21}, 0\right)$	$\left(\frac{80}{131}, \frac{15}{131}\right)$
5	$\left(\frac{15}{31}, 0\right)$	$\left(\frac{170}{271}, \frac{35}{271}\right)$

TABLE V
α and β for the Second Derivative Scheme

M	(α, β)	(α, β) (8-digit)
1	$\left(\frac{6}{15+2\pi^2}, 0\right)$	(0.17271550, 0)
2	$\left(\frac{18}{115-6\pi^2}, 0\right)$	(0.32268257, 0)
3	$\left(\frac{72}{-55+24\pi^2}, 0\right)$	(0.39588607, 0)
4	$\left(\frac{1800}{10079-600\pi^2}, 0\right)$	(0.43297984, 0)
5	$\left(\frac{900}{-977+300\pi^2}, 0\right)$	(0.45365616, 0)
1	$\frac{(832, -135+6\pi^2)}{2110+276\pi^2}$	(0.17211380, −0.01567691)
2	$\frac{(-4980+288\pi^2, 1650-180\pi^2)}{-32275+1350\pi^2+144\pi^4}$	(0.43409823, 0.02569569)
3	$\frac{(1086528-115200\pi^2, -396750+39600\pi^2)}{6486965-809136\pi^2+14400\pi^4}$	(0.52445279, 0.06147497)
4	$\frac{(-57398400+5760000\pi^2, 16791150-1710000\pi^2)}{-160987699+12661200\pi^2+360000\pi^4}$	(0.57273693, 0.08950837)
5	$\frac{(2255713800-229320000\pi^2, -632489550+63945000\pi^2)}{7752909187-873863100\pi^2+8820000\pi^4}$	(0.60066884, 0.10911819)

requires a tridiagonal solver while when $\beta \neq 0$, the scheme requires a pentadiagonal solver when inverting. It is interesting to note that as M increases, $\alpha \to 1/2$ when $\beta = 0$ and $\alpha \to 2/3$ and $\beta \to 1/6$ for both the first and second derivative schemes. These values, $(\alpha = 1/2, \beta = 0)$ and $(\alpha = 2/3, \beta = 1/6)$, as we explained in the previous section, are the solutions of the two equations, $1 - 2\alpha + 2\beta = 0$ and $-5 + 8\alpha - 2\beta = 0$, which are the conditions that the coefficients of the two highest terms in the numerator of $\mathcal{D}_l^{(1)}(\alpha, \beta)$ vanish as shown in Table II. The same values of α and β also satisfy the similar equations for the second derivative scheme. All values of α and β in Tables IV and V satisfy the necessary condition for the boundedness of the modified wavenumber, Eq. (17). Therefore, we notice that although the coefficients of the two highest terms do not completely vanish, the coefficients become very small so that $\mathcal{D}_l^{(n)}$ decays faster than before combining. The same values of α and β can be obtained through an investigation of the truncation error of the scheme.

One might suggest the optimization of α and β to minimize a certain error norm in the wavenumber space instead of maintaining the low-order truncation error. However, our scheme was derived from a spectral representation by truncation which completely spoils the order of accuracy at the low wavenumber range. Thus it appears "optimal" to impose the minimum order of accuracy using these two parameters. When $\beta = 0$ (tridiagonal system), the scheme would have the zeroth order of truncation error if the satisfaction of one optimization condition is preferred. The resulting scheme would be obviously useless. When $\beta \neq 0$ (pentadiagonal system), the second-order accuracy could be secured, allowing one optimization condition to be satisfied. However, we will not consider such a case in the present study.

Using α and β, $\mathcal{D}_l^{(1)}(\alpha, \beta)$ for a given M can be calculated. For example, when $\beta = 0$ and $M = 1$, the scheme for the first derivative becomes

$$\alpha u'_{j-1} + u'_j + \alpha u'_{j+1} = \mathcal{D}_1^{(1)}(u_{j+1} - u_{j-1}) \tag{22}$$

with $\alpha = 1/3$ and $\mathcal{D}_1^{(1)}\Delta x = 5/6$. When $\beta = 0$ and $M = 2$, the scheme becomes

$$\alpha u'_{j-1} + u'_j + \alpha u'_{j+1} = \mathcal{D}_1^{(1)}(u_{j+1} - u_{j-1}) + \mathcal{D}_2^{(1)}(u_{j+2} - u_{j-2}) \tag{23}$$

with $\alpha = 4/7$, $\mathcal{D}_1^{(1)}\Delta x = 11/14$, and $\mathcal{D}_2^{(1)}\Delta x = 1/14$. These two schemes are second-order accurate schemes, but the latter has a better wave resolution property. Similarly the fourth-order scheme can be generated by using α and β in Table IV and the corresponding coefficients in Table II.

When $\beta = 0$ and $M = 1$, the scheme for the second derivative reduces to

$$\alpha u''_{j-1} + u''_j + \alpha u''_{j+1} = \mathcal{D}_0^{(2)} u_j + \mathcal{D}_1^{(2)}(u_{j+1} + u_{j-1}) \tag{24}$$

with $\alpha = 0.17271550$, $\mathcal{D}_0^{(2)}\Delta x^2 = -2.690862$, and $\mathcal{D}_1^{(2)}\Delta x^2 = 1.345431$. When $\beta = 0$ and $M = 2$, the scheme becomes

$$\alpha u''_{j-1} + u''_j + \alpha u''_{j+1} = \mathcal{D}_0^{(2)} u_j + \mathcal{D}_1^{(2)}(u_{j+1} + u_{j-1}) + \mathcal{D}_2^{(2)}(u_{j+2} + u_{j-2}) \tag{25}$$

with $\alpha = 0.3226826$, $\mathcal{D}_0^{(2)}\Delta x^2 = -1.988295$, $\mathcal{D}_1^{(2)}\Delta x^2 = 0.7770755$, and $\mathcal{D}_2^{(2)}\Delta x^2 = 0.2170724$. The fourth-order scheme can be obtained by using α and β in Table V and the coefficients in Table III.

The modified wavenumber distributions, Eqs. (15) and (16), of our scheme (CSS) for the first and second derivatives are illustrated in Figs. 1 and 2, respectively. In each figure, the zero β case (second-order accuracy) and nonzero β case (fourth-order accuracy) are compared against the compact finite difference scheme (CS) of Lele [3] and the explicit centered difference scheme (CD) with the same stencil width. A more detailed comparison between our scheme and other optimized schemes with the same size of stencil is postponed to the next section. In all cases, the CSS shows an improved wave resolution especially in the high wavenumber region. It should be noted that although the CDs are second-, fourth-, and sixth-order accurate for $M = 1$, 2, and 3, respectively, and the CSs are fourth-, sixth-, and eighth-order accurate for $M = 1$, 2, and 3 when $\beta = 0$ while all the CSSs are second-order accurate when $\beta = 0$, the wave resolution property of the CSS is much better than that of the CS and the CD. All the CSSs show slight overshoots which are typical symptoms associated with the spectral scheme since the modified wavenumber tries to approximate a discontinuity at $\kappa = \kappa_{max}$, which is also known as the Gibbs phenomena. The improvement is more pronounced in the second derivative scheme. The fourth-order CSS (nonzero β with $M = 3$) has a significantly better wave resolution property than the tenth-order CS (nonzero β with $M = 3$).

3. COMPARISON WITH OPTIMIZED SCHEMES

Optimized schemes have been known to have good wave resolution characteristics. Among a variety of optimized schemes, compact optimized schemes have the best wave

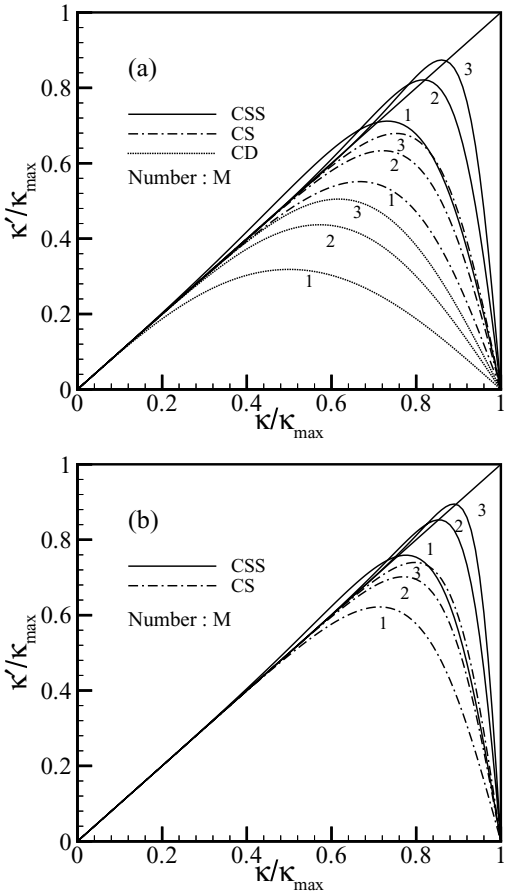

FIG. 1. Modified wavenumber distribution for the first derivative schemes: (a) dotted line, the explicit centered difference schemes (CD); chain-dotted line, the compact finite difference schemes (CS) with $\beta = 0$; solid line, the compact spectral scheme (CSS) with $\beta = 0$; (b) chain-dotted line, the CS with nonzero β; solid line, the CSS with nonzero β. The number denotes the number of terms retained in the right-hand side of the scheme, M.

resolution property. The schemes that we consider for comparison purposes are Haras and Ta'asan's [13], Kim and Lee's [14], and Gaitonde and Shang's [15] schemes. We briefly give the description of each scheme. The general forms of these schemes are

$$\beta u'_{j-2} + \alpha u'_{j-1} + u'_j + \alpha u'_{j+1} + \beta u'_{j+2} = a\frac{u_{j+1} - u_{j-1}}{2\Delta x} + b\frac{u_{j+2} - u_{j-2}}{4\Delta x} + c\frac{u_{j+3} - u_{j-3}}{6\Delta x}, \tag{26}$$

$$\beta u''_{j-2} + \alpha u''_{j-1} + u''_j + \alpha u''_{j+1} + \beta u''_{j+2} = a\frac{u_{j+l} - 2u_j + u_{j-l}}{\Delta x^2} + b\frac{u_{j+2} - 2u_j + u_{j-2}}{4\Delta x^2} + c\frac{u_{j+3} - 2u_j + u_{j-3}}{9\Delta x^2}. \tag{27}$$

The CS determines α, β, a, b, and c by enforcing the maximum possible order of truncation error to the scheme up to tenth order. Haras and Ta'asan [13] derived their schemes by minimizing the following wave resolution errors over the optimization parameter

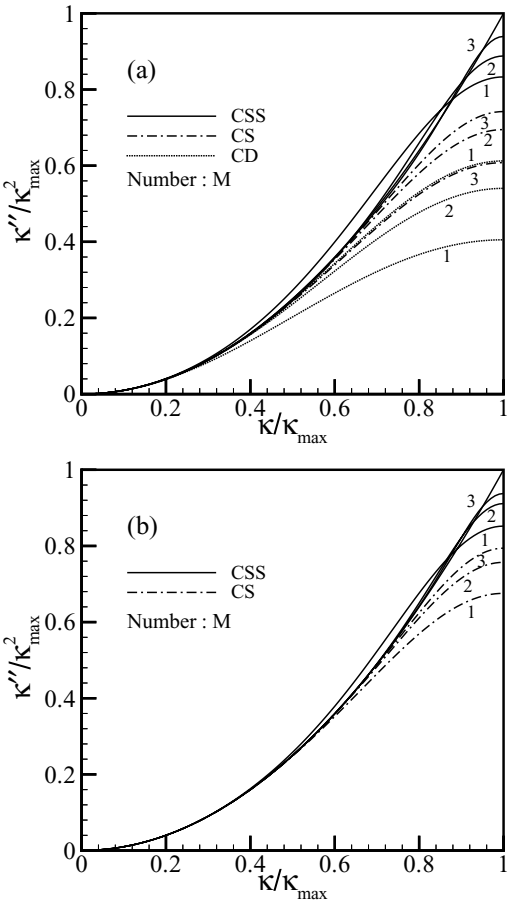

FIG. 2. Modified wavenumber distribution for the second derivative schemes: (a) dotted line, the CD; chain-dotted line, the CS with $\beta = 0$; solid line, the CSS with $\beta = 0$; (b) chain-dotted line, the CS with nonzero β; solid line, the CSS with nonzero β. The number denotes the number of terms retained in the right-hand side of the scheme, M.

space.

$$E_1(\alpha, \beta, a, b, c) = \int_0^{r\kappa_{max}} (\kappa' - \kappa)^2 W(\pi\kappa/\kappa_{max})^2 \, d\kappa \tag{28}$$

for the first derivative and

$$E_2(\alpha, \beta, a, b, c) = \int_0^{r\kappa_{max}} (\kappa'' - \kappa^2)^2 W(\pi\kappa/\kappa_{max})^2 \, d\kappa \tag{29}$$

for the second derivative, respectively, under the constraint

$$a + b + c = 1 + 2\alpha + 2\beta \tag{30}$$

to maintain the second-order accuracy. The weight function,

$$W(\omega) = e^{-n\omega^2} \tag{31}$$

was selected to approximate the function to be differentiated. r is set to 1 so that the optimization range covers the whole range of wavenumbers. Schemes with $n = 1, 2, 3$ are referred to as HT1, HT2, and HT3 and will be compared to our scheme in this study.

Kim and Lee [14] provided first derivative schemes by optimizing Eq. (28) with the choice of the weight function

$$W(\omega) = (1 + 2\alpha \cos \omega + 2\beta \cos 2\omega)e^{\omega} \tag{32}$$

and the optimization range parameter $r < 1$. The order of truncation error of their schemes ranges from second order up to eighth order depending on the choice of the number of optimization parameters. The optimum value of r for each case was sought to yield the best resolving efficiency which was defined as the range of wavenumbers over which the modified wavenumber approximates the exact wavenumber within a specified error tolerance. Note that the weight function of Haras and Ta'asan's scheme emphasizes low wavenumbers while Kim and Lee's scheme puts more weight on high wavenumbers. Kim and Lee's schemes will be referred to as KL1, KL2, KL3, and KL4 depending on the order of accuracy.

Gaitonde and Shang [15] proposed five-point compact first derivative schemes of fourth-order accuracy through optimization using several kinds of wave resolution errors. Among them, one scheme derived by consideration of stability of the full discretization including temporal integration using the fourth-order Runge–Kutta scheme is particularly interesting (CD4O6 scheme in their paper, referred to here as GS). Although the scheme was optimized for particular choices of temporal integration scheme and CFL number, the scheme provides a good wave resolution property.

The values of α, β, a, b, and c of the tested schemes (CSS, CS, GS, HT1, HT2, HT3, KL1, KL2, KL3, KL4) grouped for the same size of stencil are listed in Tables VI and VII for the first and second derivatives, respectively. Three groups under consideration are tridiagonal schemes with $\beta = c = 0$, a tridiagonal scheme with $\beta = 0$, and a full pentadiagonal scheme. The wave resolution characteristics of each scheme for the same size of stencil are compared in Figs. 3–5 for the first derivative. Compared to other schemes, our scheme has a wider range of wavenumbers over which the modified wavenumbers remain near the exact wavenumbers although an overshoot is observed. One may raise a question about the criterion of a better scheme: Is it better for a scheme to have the modified wavenumber approximating exact wavenumber over a *wide* region of wavenumbers within a relatively *large* error bound than it is to have a good approximation in a *narrow* region with a *small* error? In most applications such as turbulence or acoustic wave calculations, the energy spectrum is very flat up to the maximum wavenumber and a realization of any physical quantity is the sum of all the wavenumber components. This suggests that it is desirable for a scheme to have the wave resolution error distributed over the wavenumber space as uniformly as possible. For example, comparison of tridiagonal first derivative schemes in Figs. 3 and 4 shows that our schemes have about a 20 and 10%, respectively, wider region over which the modified wavenumbers remain near the exact wavenumbers than other optimized schemes. However, the wave resolution characteristics of full pentadiagonal schemes of CSS, HT1, KL1, and KL2 are all similar as shown in Fig. 5. For better comparison, the distribution of an error defined as $|\kappa' - \kappa|/\kappa$ is demonstrated in Figs. 6–8. It can be clearly seen that for the tridiagonal schemes, the error of our scheme is more evenly distributed than other schemes (Figs. 6 and 7) while the difference between the schemes is minor for the pentadiagonal case (Fig. 8). As will be shown in the quantitative comparison below, schemes with a

TABLE VI

Coefficients of Schemes for the First Derivative

	OT[a]	α	β	a	b	c
CSS	2	0.428571429	0	1.571428571	0.285714286	0
CS	6	0.333333333	0	1.555555556	0.111111111	0
GS	4	0.376374000	0	1.584249333	0.168498667	0
HT1	2	0.379389491	0	1.575573790	0.183205193	0
HT2	2	0.353462044	0	1.566965775	0.139958315	0
HT3	2	0.346189057	0	1.563309807	0.129068307	0
CSS	2	0.461538462	0	1.538461539	0.461538462	−0.076923077
CS	8	0.375000000	0	1.562500000	0.200000000	−0.012500000
KL1	2	0.450901855	0	1.545790417	0.434249728	−0.078236437
KL2	4	0.435181352	0	1.551941906	0.361328195	−0.042907397
KL3	6	0.408589269	0	1.568098212	0.271657107	−0.022576781
HT1	2	0.430303067	0	1.556757743	0.345162224	−0.041313832
HT2	2	0.399147627	0	1.563638637	0.256378449	−0.021721833
HT3	2	0.390409139	0	1.563888774	0.234822271	−0.017892768
CSS	4	0.581818182	0.090909091	1.296969697	1.012121212	0.036363636
CS	10	0.500000000	0.050000000	1.416666667	0.673333333	0.010000000
CS*[b]	4	0.577143900	0.089640600	1.302516600	0.993550000	0.037502450
KL1	2	0.596631925	0.103053504	1.265667929	1.079904285	0.053798648
KL2	4	0.589595521	0.097512355	1.280440844	1.049309076	0.044465832
KL3	6	0.566458285	0.081278202	1.323482375	0.944394243	0.027596356
KL4	8	0.537265947	0.064906379	1.377189728	0.814447053	0.016707870
HT1	2	0.577940367	0.089014348	1.303026954	0.994883769	0.035998707
HT2	2	0.580181893	0.087728489	1.305894194	0.997588496	0.032338072
HT3	2	0.582114374	0.086722408	1.308673396	0.999090689	0.029909479

[a] Order of truncation error.

[b] Spectral-like compact finite difference scheme.

TABLE VII

Coefficients of Schemes for the Second Derivative

	OT[a]	α	β	a	b	c
CSS	2	0.322682570	0	0.777075611	0.868289511	0
CS	6	0.181818182	0	0.109090909	0.272727273	0
HT1	2	0.228565761	0	1.013953841	0.443177681	0
HT2	2	0.202815007	0	1.059813517	0.345816497	0
HT3	2	0.195277077	0	1.071669507	0.318884646	0
CSS	2	0.395886070	0	0.499643999	1.518987289	−0.226859144
CS	8	0.236842105	0	0.967105263	0.536842105	−0.030263158
HT1	2	0.312517607	0	0.770135200	0.946957741	−0.092057727
HT2	2	0.270248861	0	0.886352558	0.706517264	−0.052372100
HT3	2	0.258069915	0	0.917032274	0.642533098	−0.043425541
CSS	4	0.524452790	0.061474970	0.149004128	1.822086913	0.200764495
CS	10	0.371523916	0.023915462	0.592324805	1.154616240	0.043937709
CS*[b]	4	0.502092660	0.055691690	0.215649350	1.723322000	0.176597300
HT1	2	0.502475058	0.055444067	0.215053644	1.724652314	0.176132291
HT2	2	0.504158207	0.052758536	0.212046571	1.748840994	0.152945921
HT3	2	0.505398637	0.051244445	0.211225610	1.760957934	0.141102660

[a] Order of truncation error.

[b] Spectral-like compact finite difference scheme.

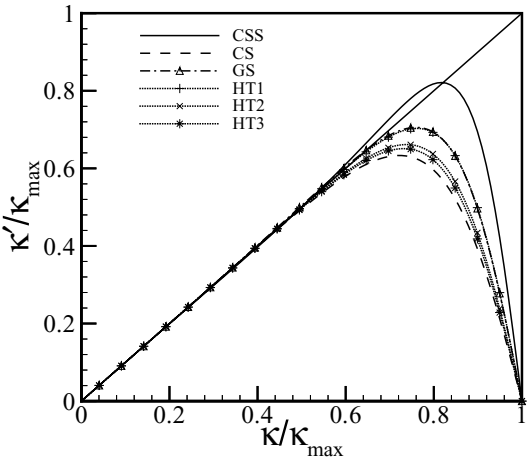

FIG. 3. Modified wavenumber distribution for the tridiagonal first derivative schemes with $\beta = c = 0$: solid line, CSS; dashed line, CS; chain-dotted line, GS; dotted lines, HTn.

wider range of wavenumbers over which the modified wavenumbers approximate exact wavenumbers with a large error bound perform better than schemes with opposite wave resolution characteristics.

For the second derivate, the modified wavenumber distributions for our scheme, compact difference scheme, and HTn are shown in Figs. 9–11. From the same point of view, our second derivative schemes have a much better wave resolution property than other optimized schemes for all sizes of stencil as shown in Figs. 9–11. This can be attributed to the fact that the pseudospectral representation for the second derivative has faster convergence than that for the first derivative. Recall that our schemes were derived not by optimizing any prescribed wave resolution error, but by a pure truncation of pseudospectral representation and imposition of low-order accuracy.

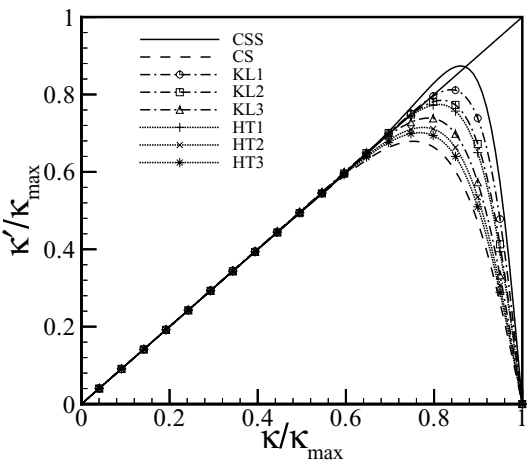

FIG. 4. Modified wavenumber distribution for the tridiagonal first derivative schemes with $\beta = 0$: solid line, CSS; dashed line, CS; chain-dotted lines, KLn; dotted lines, HTn.

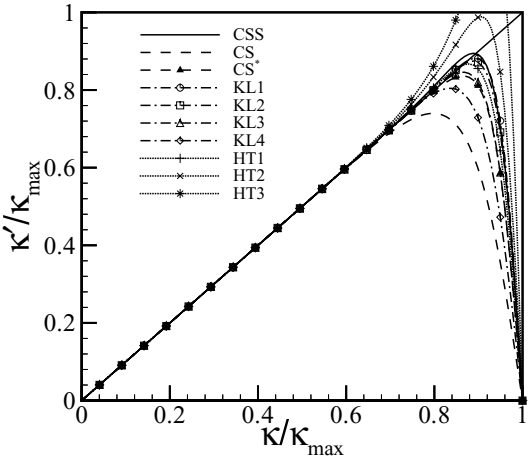

FIG. 5. Modified wavenumber distribution for the pentadiagonal first derivative schemes: solid line, CSS; dashed lines, CS; chain-dotted lines, KLn; dotted lines, HTn.

To quantitatively compare the wave resolution capability, we consider an error defined as follows. The energy spectrum of three-dimensional isotropic turbulence decays as $\sim\kappa^{-5/3}$ in the inertial range. The extent to which a scheme resolves such a spectrum can be measured by the following definition of error suggested by [22]

$$\text{Error}^{(1)} \equiv \frac{\int_{\kappa=0}^{\kappa_{max}} |\kappa' - \kappa| E(\kappa)\, d\kappa}{\int_{\kappa=0}^{\kappa_{max}} \kappa E(\kappa)\, d\kappa}, \tag{33}$$

$$\text{Error}^{(2)} \equiv \frac{\int_{\kappa=0}^{\kappa_{max}} |\kappa'' - \kappa^2| E(\kappa)\, d\kappa}{\int_{\kappa=0}^{\kappa_{max}} \kappa^2 E(\kappa)\, d\kappa} \tag{34}$$

for the first and second derivative schemes, respectively. Here, $E(\kappa) = C\kappa^{-5/3}$ and this

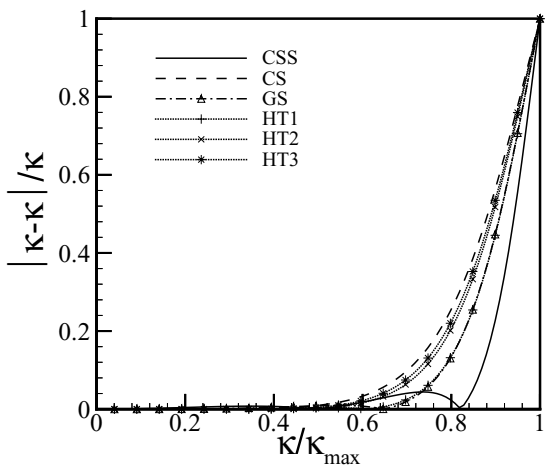

FIG. 6. Modified wavenumber error distribution for the tridiagonal first derivative schemes with $\beta = c = 0$: solid line, CSS; dashed line, CS; chain-dotted line, GS; dotted lines, HTn.

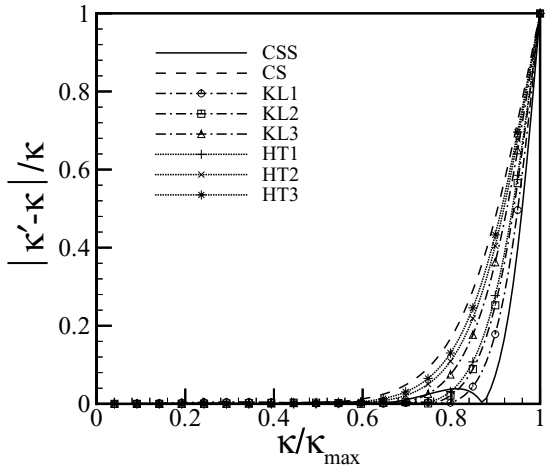

FIG. 7. Modified wavenumber error distribution for the tridiagonal first derivative schemes with $\beta = 0$: solid line, CSS; dashed line, CS; chain-dotted lines, KL*n*; dotted lines, HT*n*.

kind of error is quite effective in the evaluation of schemes having potential use in LES. The errors of the CSS are listed in Tables VIII and IX compared with the CS, GS, KLn, HT*n* for the first and second derivative schemes, respectively. For the same stencil width, the smallest error among each group is indicated by an underscore. Among the tridiagonal first derivative schemes, our scheme has the smallest error. Comparison between the pentadiagonal schemes reveals that the error of KL1 is the smallest, but the errors of our scheme and HT are comparative. It should be noted that the modified wavenumber for HT2 has a large overshoot (Fig. 5), which obviously does not spoil the resolution error. This suggests that an overshoot is not harmful. It might impose a little more of a strict time step restriction in an explicit temporal integration. As expected, our second derivative schemes outperform all other schemes quite significantly as shown in Table IX.

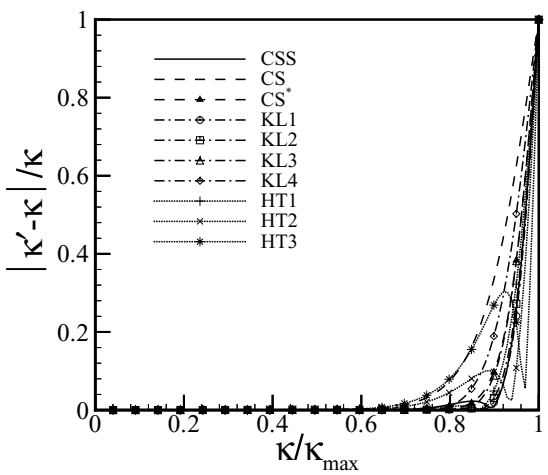

FIG. 8. Modified wavenumber error distribution for the pentadiagonal first derivative schemes: solid line, CSS; dashed lines, CS; chain-dotted lines, KL*n*; dotted lines, HT*n*.

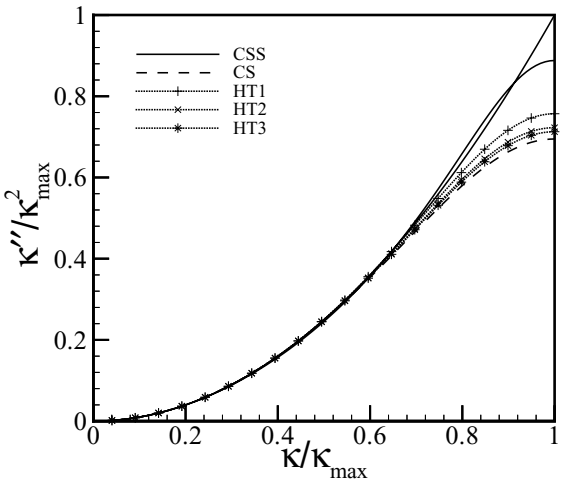

FIG. 9. Modified wavenumber distribution for the tridiagonal second derivative schemes with $\beta = c = 0$: solid line, CSS; dashed line, CS; dotted lines, HTn.

The best way to investigate the performance of a scheme is to directly apply the scheme to calculate derivatives of a known function. We select a function that decays very slowly in the wavenumber space

$$u(x) = \sum_{\kappa=1}^{49} \kappa^{-n} \cos(\kappa x + \psi_\kappa) \tag{35}$$

in the periodic domain, $0 \le x \le 2\pi$, and ψ_κ is a random phase. n is chosen to be very low, $n = 0, 1, 2$. This simulates a typical spectrum of the velocity in turbulence in the inertial

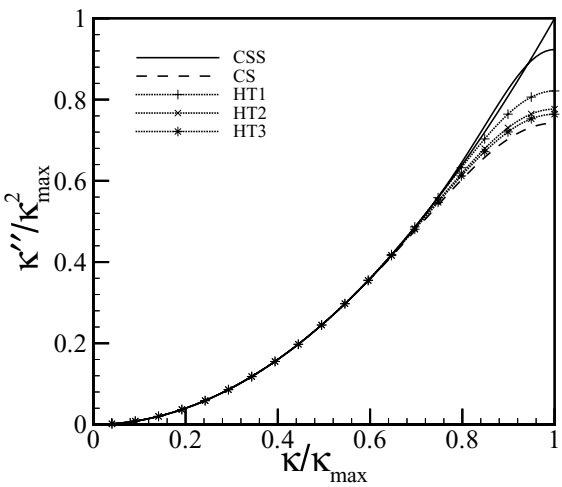

FIG. 10. Modified wavenumber distribution for the tridiagonal second derivative schemes with $\beta = 0$: solid line, CSS; dashed line, CS; dotted lines, HTn.

TABLE VIII
Wave Resolution Error Defined in Eq. (33)

Scheme	Tridiagonal ($\beta = c = 0$)	Tridiagonal ($\beta = 0$)	Pentadiagonal
CSS	0.03536	0.02438	0.01763
CS	0.06532	0.05299	0.03895
CS*			0.02208
GS	0.04883		
KL1		0.02848	0.01654
KL2		0.03233	0.01759
KL3		0.04049	0.02166
KL4			0.02802
HT1	0.04817	0.03374	0.01937
HT2	0.05754	0.04462	0.01853
HT2	0.06032	0.04766	0.02513

TABLE IX
Wave Resolution Error Defined in Eq. (34)

Scheme	Tridiagonal ($\beta = c = 0$)	Tridiagonal ($\beta = 0$)	Pentadiagonal
CSS	0.01909	0.00859	0.00431
CS	0.06277	0.04382	0.02751
CS*			0.00760
HT1	0.03693	0.01942	0.00653
HT2	0.05004	0.03172	0.00865
HT2	0.05441	0.03588	0.01675

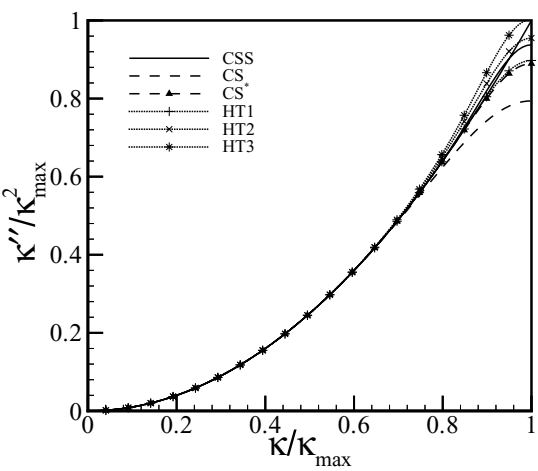

FIG. 11. Modified wavenumber distribution for the pentadiagonal second derivative schemes: solid line, CSS; dashed lines, CS; dotted lines, HT*n*.

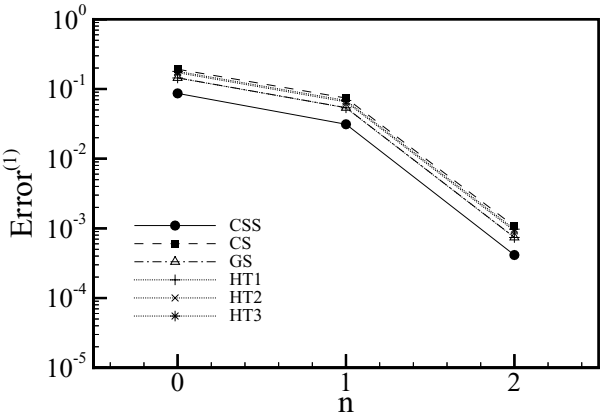

FIG. 12. The error defined by Eq. (36) for the tridiagonal first derivative schemes with $\beta = c = 0$: solid line, CSS; dashed line, CS; chain-dotted line, GS; dotted lines, HTn.

range. Δx is set to $2\pi/100$, meaning that the grid is intentionally chosen to be marginal. We apply our scheme, compact scheme, optimized compact schemes to obtain the first and second derivatives and compare the error defined as

$$E^{(1)} = \frac{\sum_{j=1}^{100}(u'(x_j) - u'_j)^2\,\Delta x}{\sum_{j=1}^{100}(u'(x_j))^2\,\Delta x} \tag{36}$$

$$E^{(2)} = \frac{\sum_{j=1}^{100}(u''(x_j) - u''_j)^2\,\Delta x}{\sum_{j=1}^{100}(u''(x_j))^2\,\Delta x}, \tag{37}$$

where $u'(x_j), u''(x_j)$ denote the exact derivatives and u'_j, u''_j denote the numerical estimates, respectively. The errors for $n = 0, 1, 2$ for the first and second derivatives are illustrated in Figs. 12–14 and 15–17, respectively. For the first derivative, our scheme produces the most accurate solution for a nondecaying function ($n = 0$) and slowly decaying functions ($n = 1, 2$) when using the tridiagonal schemes. When $n = 3$ or $n = 4$, the trend is

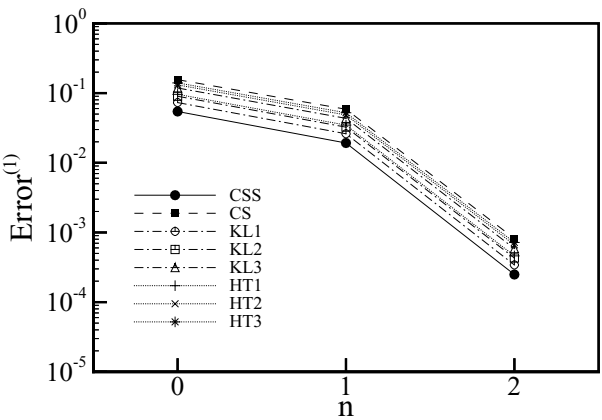

FIG. 13. The error defined by Eq. (36) for the tridiagonal first derivative schemes with $\beta = 0$: solid line, CSS; dashed line, CS; chain-dotted lines, KLn; dotted lines, HTn.

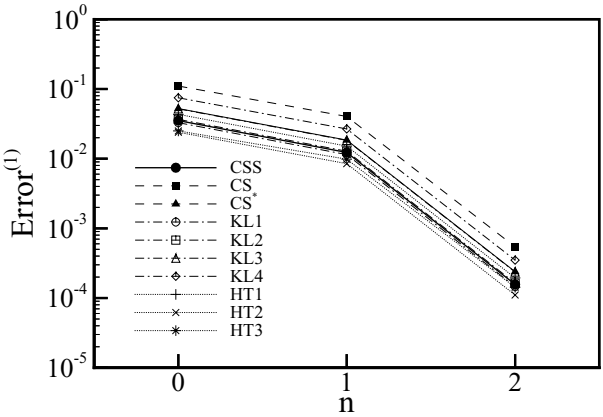

FIG. 14. The error defined by Eq. (36) for the pentadiagonal first derivative schemes: solid line, CSS; dashed lines, CS; chain-dotted lines, KLn; dotted lines, HTn.

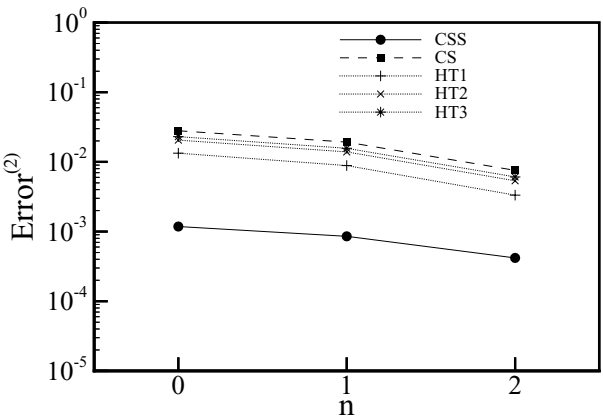

FIG. 15. The error defined by Eq. (37) for the tridiagonal second derivative schemes with $\beta = c = 0$: solid line, CSS; dashed line, CS; dotted lines, HTn.

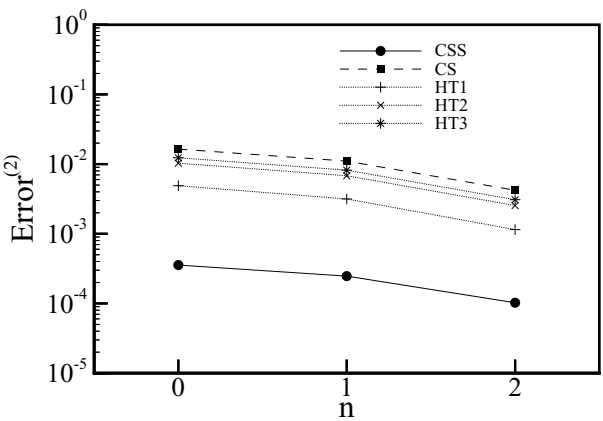

FIG. 16. The error defined by Eq. (37) for the tridiagonal second derivative schemes with $\beta = 0$: solid line, CSS; dashed line, CS; dotted lines, HTn.

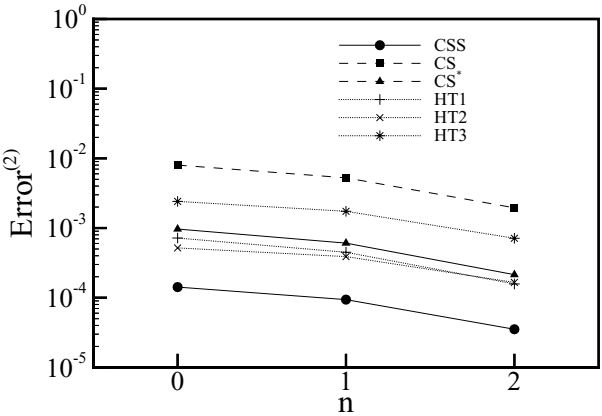

FIG. 17. The error defined by Eq. (37) for the pentadiagonal second derivative schemes: solid line, CSS; dashed lines, CS; dotted lines, HTn.

similar (figure not shown). Among the pentadiagonal schemes, the calculation by HT2 is the best, then our scheme, and KL1 following. For the second derivative calculation, however, our scheme yields the most accurate result for both the tridiagonal and pentadiagonal schemes, the error being smaller by one or two orders of magnitude than other schemes.

In summary, from comparison of the wave resolution, the prescribed error, and tests of schemes to real functions, it is clear that our scheme for the first derivative performs better than any other scheme when the tridiagonal schemes are used. The performance of the pentadiagonal schemes is all comparative. For the second derivative, however, our schemes produce the best estimation for all sizes of stencil. This suggests that an optimization in the wavenumber space minimizing a prescribed error does not guarantee the best performance unless the cost function to be minimized is carefully selected.

4. BOUNDARY SCHEMES

4.1. First Derivative Scheme

For the calculation of derivatives at the boundary, special attention should be paid since the function values beyond the boundary are not available. First, we consider the following scheme for the first derivative at the boundary, u'_0.

$$u'_0 + \alpha u'_1 + \beta u'_2 = \mathcal{D}_0^{(1)} u_0 + \sum_{j=1}^{M} \mathcal{D}_j^{(1)} u_j, \tag{38}$$

where $\mathcal{D}_j^{(1)}$, $j = 1, \ldots, M$ are functions of α and β only and can be constructed using Eq. (11). Here again, the series is truncated after the coefficients are rearranged. $\mathcal{D}_0^{(1)}$ has a nonzero value due to the asymmetry of the scheme, but the value is modified to be $-\sum_{j=1}^{M} \mathcal{D}_j^{(1)}$ for the shift invariance. This modification has no rational background but guarantees the most basic property without introducing one more degree of freedom. To

determine α and β, we investigate the wave resolution property of the scheme. This time, the modified wavenumber becomes a complex number and the following condition is imposed for the unique determination of α when β is set to zero.

$$\text{Real part}\left(\frac{d(\kappa'/\kappa_{max})}{d(\kappa/\kappa_{max})}\right)_{\kappa=0} = 1, \tag{39}$$

the condition for the imaginary part being satisfied automatically since one degree of freedom is enough to ensure the first-order accuracy. For the determination of α and β together, the following extra condition is used.

$$\text{Imaginary part}\left(\frac{d^2(\kappa'/\kappa_{max})}{d(\kappa/\kappa_{max})^2}\right)_{\kappa=0} = 0, \tag{40}$$

where the accompanying condition for the real part is automatically satisfied, implying that the second-order accuracy is guaranteed. We find that when β is set to zero, $\alpha = 0$ for $M = 1$, $\alpha = 1$ for $M = 2$, and $\alpha = 0$ for $M = 3$. When $M = 1$, the scheme reduces to the first-order explicit forward-difference scheme, and when $M = 2$, the modified wavenumber becomes unbound at the maximum wavenumber. With $M = 3$, the wave resolution becomes too poor to be useful.

Investigation of the second-order scheme (nonzero β case) reveals that $\alpha = 3$, $\beta = 1$ for $M = 2$ and $\alpha = 4$, $\beta = 2$ for $M = 3$. The wave resolution of $M = 2$ case is relatively good, but the scheme is exactly the same as the interior scheme for u'_1 with $M = 1$. Therefore, both schemes cannot be used together to obtain the first derivative of a given function since the corresponding matrix becomes singular. The second scheme with $M = 3$ is also not useful since the scheme is found to be unstable when applied to a simple one-dimensional wave equation. In summary, we could not find a useful boundary scheme in this approach if we exclude a simple explicit forward-difference scheme which has not good wave resolution property. The reason for the failure probably lies in the fact that only half side expansion is considered in the derivation.

We take another approach by including a ghost data point located outside the boundary. The expression for the first derivative at the boundary then becomes

$$u'_0 + \alpha u'_1 + \beta u'_2 = \mathcal{D}^{(1)}_{-1} u_{-1} + \mathcal{D}^{(1)}_0 u_0 + \sum_{j=1}^{M} \mathcal{D}^{(1)}_j u_j, \tag{41}$$

where $\mathcal{D}^{(1)}_j$, $j = 1, \ldots, M$ are constructed using Eq. (11). Since u_{-1} is not available, we use the first-order extrapolation when β is set to zero and the second-order extrapolation when β is not zero. These extrapolations are reasonable since the scheme itself has the same order of accuracy for each case. Then the scheme has the same form as Eq. (38) with $\mathcal{D}^{(1)}_0$ and $\mathcal{D}^{(1)}_1$ modified when using the first-order extrapolation and $\mathcal{D}^{(1)}_0$, $\mathcal{D}^{(1)}_1$, and $\mathcal{D}^{(1)}_2$ modified for the second-order extrapolation. After that, the shift-invariance condition is imposed on $\mathcal{D}^{(1)}_0$; i.e., $\mathcal{D}^{(1)}_0 = -\sum_{j=1}^{M} \mathcal{D}^{(1)}_j$. The resulting expressions for $\mathcal{D}^{(1)}_1$ are presented in Table X. The values for α and β obtained from the conditions, Eqs. (39) and (40), are shown together. When β is set to zero, $\alpha = 0$ for $M = 2$ and $\alpha = 1$ for $M = 3$. These two cases are not useful since the first scheme is just a first-order explicit scheme using three function values, which is no better than the first-order forward-difference

TABLE X
α, β, and $\mathcal{D}_j^{(1)}$ for the Boundary Scheme

α	β	M	$\mathcal{D}_1^{(1)}\Delta x$	$\mathcal{D}_2^{(1)}\Delta x$	$\mathcal{D}_3^{(1)}\Delta x$
$\frac{2}{3}$	0	1	$2-\frac{\alpha}{2}$		
$\frac{20}{9}$	$\frac{2}{3}$	2	$4-\frac{3\alpha}{2}$	$-\frac{3}{2}+\frac{3\alpha}{2}-\frac{\beta}{3}$	
$\frac{7}{3}$	1	3	$4-\frac{3\alpha}{2}$	$-\frac{3}{2}+\frac{3\alpha}{2}-\frac{\beta}{3}$	$\frac{1}{3}-\frac{\alpha}{2}+\beta$

scheme, and the second scheme has the modified wavenumber unbounded at the maximum wavenumber. Therefore, these two schemes are not included in the table. The modified wavenumber distribution for the boundary schemes is shown in Fig. 18. The real and imaginary parts of the modified wavenumber for the first-order accurate scheme with $\beta = 0$ and

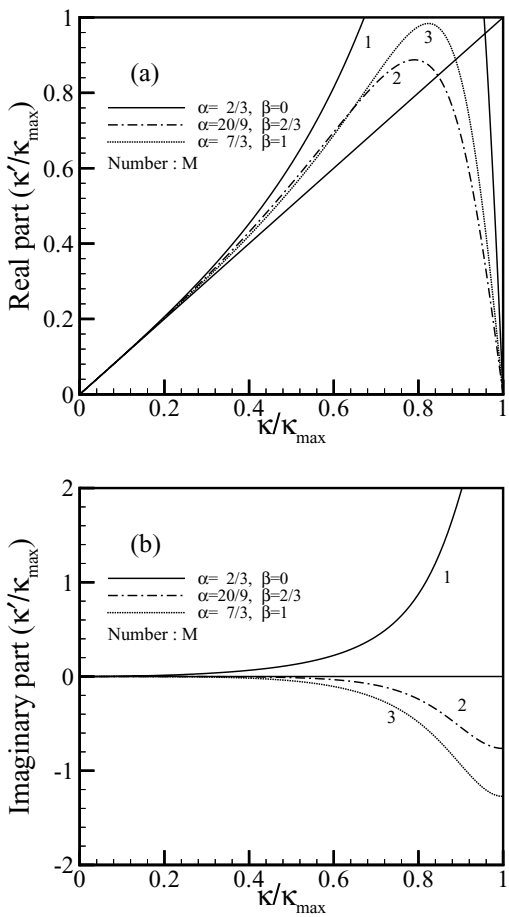

FIG. 18. Modified wavenumber for the first derivative boundary schemes: (a) the real part, solid line, $\alpha = 2/3$, $\beta = 0$, $M = 1$; chain-dotted line, $\alpha = 20/9$, $\beta = 2/3$, $M = 2$; dotted line, $\alpha = 7/3$, $\beta = 1$, $M = 3$; (b) the imaginary part, solid line, $\alpha = 2/3$, $\beta = 0$, $M = 1$; chain-dotted line, $\alpha = 20/9$, $\beta = 2/3$, $M = 2$; dotted line, $\alpha = 7/3$, $\beta = 1$, $M = 3$.

$M = 1$ show large error. The second-order scheme with $\alpha = 20/9$ and $\beta = 2/3$, $M = 2$ is recommended.

4.2. Stability Analysis

In this section, we investigate the stability characteristics of the boundary schemes introduced in the previous section by applying them along with a choice of the interior scheme to the computation of the one-dimensional wave equation

$$\frac{\partial u}{\partial t} + c\frac{\partial u}{\partial x} = 0 \tag{42}$$

in the domain, $0 \le x \le 1$, with the boundary condition, $u(0, t) = 0$. $x_j = j\Delta x$, $j = 0, \ldots, N$ with $\Delta x = 1/N$. If using the interior and boundary schemes for the first derivative, we obtain the following matrix equation for the discretized variable, $u_j(t)$, $j = 1, \ldots, N$.

$$\Delta x A_{jk} u'_k(t) = B_{jk} u_k(t), \tag{43}$$

where A_{jk}, B_{jk} are $N \times N$ matrices and the prime denotes differentiation with respect to x. The boundary condition, $u_0 = 0$, is enforced by the boundary scheme from which u'_0 is evaluated and used in the interior scheme at $j = 1$. The discretized form of Eq. (42) then becomes

$$\Delta x A_{jk} \frac{du_k}{dt} = -c B_{jk} u_k. \tag{44}$$

Using a normal mode, $u_j(t) = \hat{u}_j \exp(\omega t)$, we obtain an eigenvalue relation,

$$\omega' A_{jk} \hat{u}_k = B_{jk} \hat{u}_k \tag{45}$$

with the eigenvalue, $\omega' = -\omega \Delta x / c$. With the interior scheme fixed ($\beta = 0$, $M = 1$ case), we examine the eigenvalues for the three boundary schemes introduced in the previous section. Figure 19 shows the eigenvalue distributions for the three boundary schemes for several N's. The real parts of all the eigenvalues are negative, indicating stability. As N increases, the real part of the eigenvalue approaches the imaginary axis. We also tested all combinations of the interior and boundary scheme for stability and found that no positive real part of the eigenvalue is observed.

4.3. Second Derivative Scheme

An analogous derivation of the second derivative boundary scheme is possible. For the second derivative at the boundary node, u''_0, we consider the following form.

$$u''_0 + \alpha u''_1 + \beta u''_2 = \mathcal{D}_0^{(2)} u_0 + \sum_{j=1}^{M} \mathcal{D}_j^{(2)} u_j, \tag{46}$$

where $\mathcal{D}_j^{(2)}$, $j = -1, \ldots, M$ are constructed using Eq. (12) and $\mathcal{D}_0^{(2)} = -\sum_{j=1}^{M} \mathcal{D}_j^{(2)}$ for the shift invariance. The following conditions are imposed for the unique determination of α and β.

$$\text{Imaginary part}\left(\frac{d(\kappa''/\kappa_{max})}{d(\kappa/\kappa_{max})}\right)_{\kappa=0} = 0 \tag{47}$$

$$\text{Real part}\left(\frac{d^2(\kappa''/\kappa_{max})}{d(\kappa/\kappa_{max})^2}\right)_{\kappa=0} = 2 \tag{48}$$

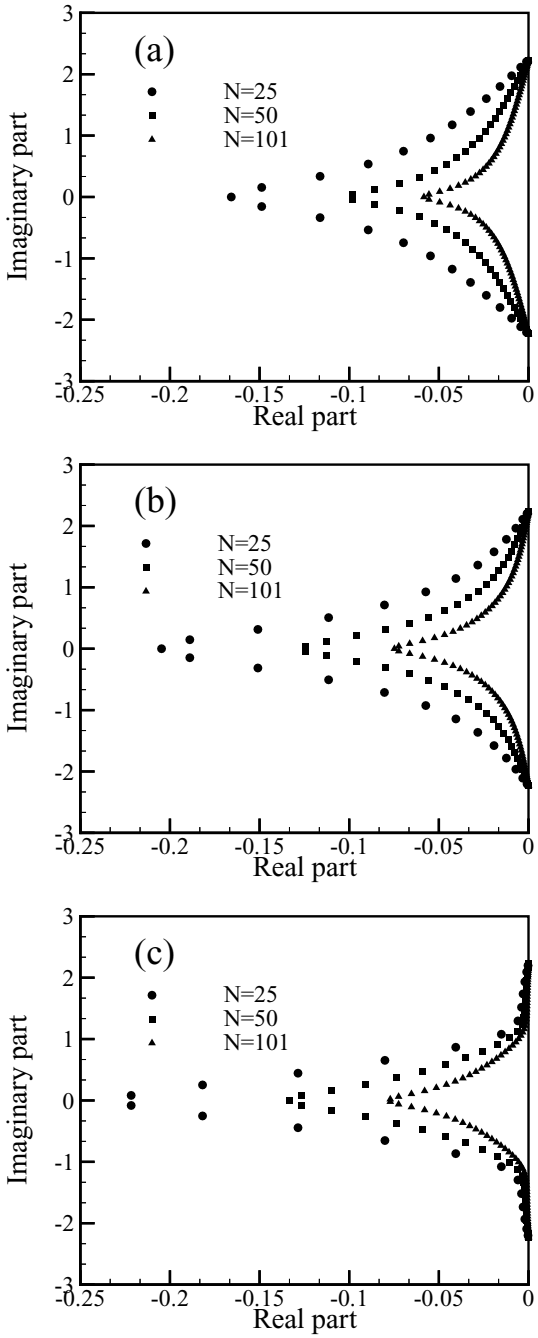

FIG. 19. Eigenvalue spectrum ω' of Eq. (45) for three boundary schemes: (a) $\alpha = 2/3$, $\beta = 0$, $M = 1$; (b) $\alpha = 20/9$, $\beta = 2/3$, $M = 2$; (c) $\alpha = 7/3$, $\beta = 1$, $M = 3$. N denotes the number of grid points.

with the accompanying conditions satisfied automatically. Therefore, the second-order accuracy is guaranteed. The corresponding values for α, β, and $\mathcal{D}_j^{(2)}$ are listed in Table XI. When β is set to zero, the first-order accurate schemes can be derived. However, these schemes show a very poor wave resolution performance. Thus we present the second-order

TABLE XI
α, β, and $\mathcal{D}_j^{(2)}$ for the Boundary Scheme

α	β	M	$\mathcal{D}_1^{(2)}\Delta x^2$	$\mathcal{D}_2^{(2)}\Delta x^2$	$\mathcal{D}_3^{(2)}\Delta x^2$
$\frac{-18+12\pi^2}{-54-3\pi^2+\pi^4}$	$\frac{126-9\pi^2}{2(-54-3\pi^2+\pi^4)}$	2	$2-\frac{\pi^2}{3}\alpha+2\beta$	$-\frac{1}{2}+2\alpha-\frac{\pi^2}{3}\beta$	
$\frac{-216+16\pi^2}{297-51\pi^2+2\pi^4}$	$\frac{18-4\pi^2}{297-51\pi^2+2\pi^4}$	3	$2-\frac{\pi^2}{3}\alpha+2\beta$	$-\frac{1}{2}+2\alpha-\frac{\pi^2}{3}\beta$	$\frac{2}{9}-\frac{\alpha}{2}+2\beta$

schemes with nonzero β only. The wave resolutions for the second-order accurate schemes are shown in Fig. 20. The imaginary part almost vanishes for both schemes.

The boundary schemes for the first and second derivatives we derived are at most second-order accurate while the wave resolution of these schemes is much better than the explicit scheme or the CS of higher order.

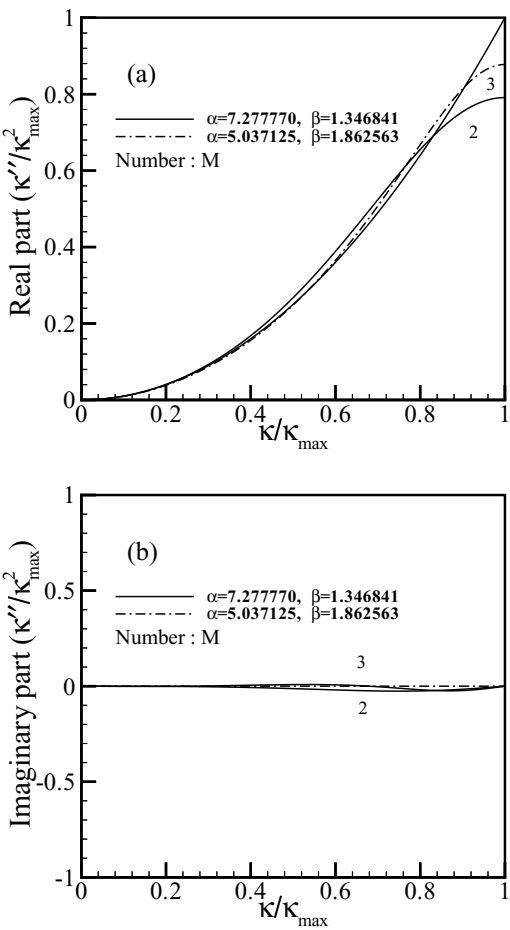

FIG. 20. Modified wavenumber for the second derivative boundary schemes: (a) the real part, solid line, $\alpha = 7.277770$, $\beta = 1.346841$, $M = 2$; chain-dotted line, $\alpha = 5.037125$, $\beta = 1.862563$, $M = 3$; (b) the imaginary part, solid line, $\alpha = 7.277770$, $\beta = 1.346841$, $M = 2$; chain-dotted line, $\alpha = 5.037125$, $\beta = 1.862563$, $M = 3$.

5. ILLUSTRATIVE EXAMPLE

5.1. Forced Solution of Three-Dimensional Isotropic Turbulence

To evaluate the capability of the proposed scheme in predicting three-dimensional turbulence, a forced isotropic homogeneous turbulence in a three-dimensional periodic domain was simulated using the CSS, CS, KL1, and HT1 as well as a spectral method. The Navier–Stokes equation with nonlinear terms written in a rotational form with a forcing reads

$$\frac{\partial \mathbf{u}}{\partial t} = \mathbf{u} \times \boldsymbol{\omega} - \nabla p + \nu \nabla^2 \mathbf{u} + \mathbf{f}, \tag{49}$$

where $\mathbf{u}$, ω, p, and ν denote velocity, vorticity, pressure, and viscosity, respectively. Periodicity of the variables in all three directions was assumed in a box of $2\pi \times 2\pi \times 2\pi$. $\mathbf{f}$ is a forcing satisfying $\nabla \cdot \mathbf{f} = 0$ given by

$$f_x = A \sin y \sin z, \tag{50}$$

$$f_y = A \sin z \sin x, \tag{51}$$

$$f_z = A \sin x \sin y, \tag{52}$$

with the forcing amplitude A. This large-scale forcing maintains statistically stationary turbulence. Then the Kolmogorov scaling relation for the energy spectrum can be expected in the inertial range for high Reynolds numbers. For the temporal integration of the nonlinear terms and forcing, the second-order Adams–Bashforth method was adopted while the viscous terms were integrated using the Crank–Nicolson method. All the temporal integrations were carried out in the Fourier space and the nonlinear terms were computed in the physical space. Dealiasing was carried out in all computations to compare the scheme's performance in the absence of the aliasing error. Otherwise the aliasing error would spoil high wavenumber components, especially when the rotational form of the nonlinear term is used. Although dealiasing in the applications of compact schemes in a nonperiodic situation is impossible, our aim in this study is to compare the CSS and other optimized schemes to the reference scheme, the spectral method. The performances of the tridiagonal schemes are investigated through comparison with a spectral scheme. The CSS, CS, and HT1 with $\beta = c = 0$ for the first and second derivatives were selected. Since Kim and Lee [14] did not provide schemes for the second derivative, the first derivative scheme was twice applied to calculate the second derivative. Furthermore, the KL1 with a wider stencil ($\beta = 0, c \neq 0$) was chosen. The resolution used was 64^3.

Due to isotropy, the turbulent energy dissipation rate, ϵ, can be estimated by

$$\epsilon = 15\nu \left\langle \left(\frac{\partial u_1}{\partial x_1} \right)^2 \right\rangle, \tag{53}$$

where the bracket denotes averaged quantity. From this, the Taylor microscale, λ, was calculated by

$$\lambda = \left(\frac{15\nu u'^2}{\epsilon} \right)^{1/2}, \tag{54}$$

TABLE XII
Computed Turbulence Statistics

Scheme	Re_λ	u'	ϵ	λ	η
SS[a]	70.56	0.666	0.372	0.169	0.0102
CSS	70.95	0.634	0.302	0.178	0.0108
CS	59.95	0.563	0.271	0.167	0.0110
KL1	59.56	0.610	0.369	0.155	0.0102
HT1	61.59	0.602	0.327	0.163	0.0105

[a] Spectral scheme.

where $u' = (2k/3)^{1/2}$. Here, $k = 1/2(\langle u_1^2\rangle + \langle u_2^2\rangle + \langle u_3^2\rangle)$. Computed values of $\mathrm{Re}_\lambda (\equiv u'\lambda/\nu)$, u', ϵ, λ, and the Kolmogorov length scale $\eta (\equiv \nu^{3/4}\epsilon^{-1/4})$ for each scheme are listed in Table XII. Dimensional quantities are normalized in such a way that the forcing amplitude $2A = 1.0$ and the computational domain $L_x = 2\pi$. Although all simulations were carried out under the same conditions, turbulence statistics are quite differently estimated. The fluctuation velocity and dissipation rate are underestimated by all the schemes tested compared to the exact value obtained by the spectral scheme. Note that $\Delta x (=2\pi/64)$ is about 10 times larger than the Kolmogorov length scale, meaning marginal resolution.

To investigate the wave resolution performance, the one-dimensional energy spectra, $E_{11}(\kappa_1)$, defined as

$$E_{11}(\kappa_1) \equiv \frac{1}{d\kappa_1} \sum_{\kappa_2} \sum_{\kappa_3} \sum_{i=1}^{3} |\hat{u}_i(\kappa_1, \kappa_2, \kappa_3)|^2 \tag{55}$$

for the spectral scheme, CSS, CS, KL1, and HT1 are compared in Fig. 21. $\hat{u}_i(\kappa_1, \kappa_2, \kappa_3)$ is the Fourier coefficient of velocity. Here, the mean part of the solution, i.e., $(u_1(0, \kappa_2, \kappa_3)$,

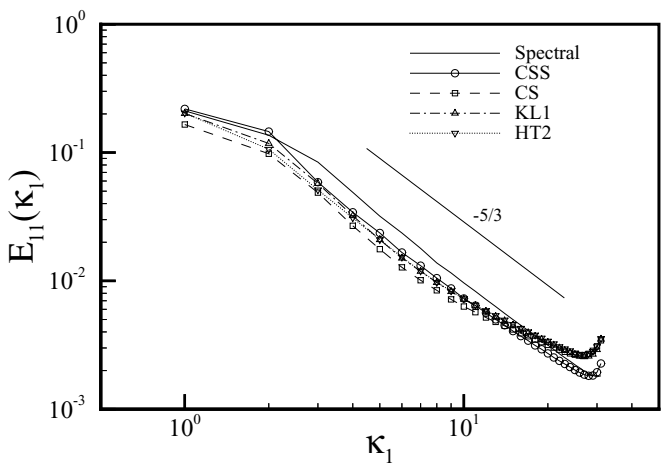

FIG. 21. One-dimensional energy spectra, $E_{11}(\kappa_1)$, obtained by the schemes tested: solid line without symbol, spectral scheme; solid line, CSS; dashed line, CS; chain-dotted line, KL1; dotted line, HT2.

$u_2(\kappa_1, 0, \kappa_3)$, $u_3(\kappa_1, \kappa_2, 0)$), is not included. For isotropic turbulence, the energy spectrum, $E(\kappa)$, behaves as

$$E(\kappa) = C\epsilon^{2/3}\kappa^{-5/3} \tag{56}$$

in the inertial range. Here C is the Kolmogorov constant and $\kappa = \sqrt{\kappa_1^2 + \kappa_2^2 + \kappa_3^2}$. In isotropic turbulence the one-dimensional spectra are determined by the energy spectrum as [23]

$$E_{11} = \int_{\kappa_1}^{\infty} \frac{E(\kappa)}{\kappa}\left(1 - \frac{\kappa_1^2}{\kappa^2}\right) d\kappa. \tag{57}$$

This allows $E_{11}(\kappa_1)$ to be written as

$$E_{11}(\kappa_1) = \frac{18}{55} C\epsilon^{2/3}\kappa_1^{-5/3}. \tag{58}$$

It is shown that the spectral method produces correct inertial range scaling. However, decaying behavior in the viscous range is not observed owing to the use of marginal resolution. Compared to the CS, KL1, and HT1, our scheme yields better behavior of the energy spectrum in that the slope is relatively well predicted and the spectrum does not show an energy pile-up near the maximum wavenumber. Differences between the schemes are more pronounced in the plot of $\epsilon^{-2/3}\kappa_1^{5/3}E_{11}(\kappa_1)$ as shown in Fig. 22. The spectral solution and CSS show a plateau region whereas the CS, KL1, and HT1 do not capture the inertial range scaling well. The CS, KL1, and HT1 underpredict large-scale motion and overpredict small-scale motion, resulting in lower values of u' as shown in Table XII. For the same reason, the dissipation rate emphasizing the high wavenumber components predicted by KL1 or HT1 rather approaches the exact value.

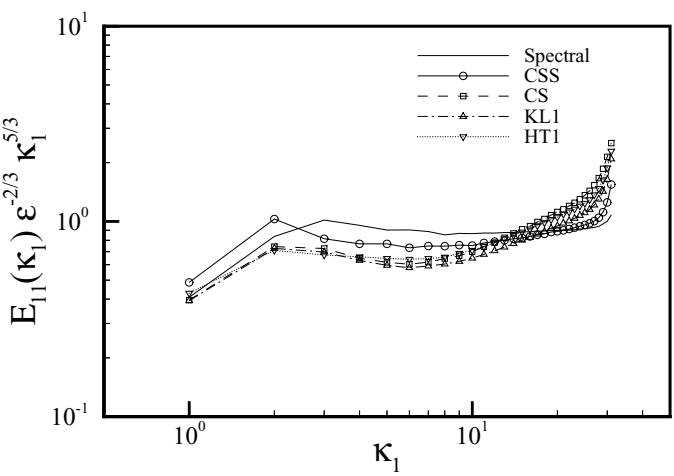

FIG. 22. Scaled one-dimensional energy spectra, $E_{11}(\kappa_1)\epsilon^{-2/3}\kappa_1^{5/3}$, obtained by the schemes tested: solid line without symbol; solid line, CSS; dashed line, CS; chain-dotted line, KL1; dotted line, HT1.

The wave resolving performance of a scheme in predicting vorticity components can be examined through the one-dimensional enstrophy spectrum defined as

$$E_{11}^{\omega}(\kappa_1) \equiv \frac{1}{d\kappa_1} \sum_{\kappa_2} \sum_{\kappa_3} \sum_{i=1}^{3} |\hat{\omega}_i(\kappa_1, \kappa_2, \kappa_3)|^2, \tag{59}$$

where $\hat{\omega}_i(\kappa_1, \kappa_2, \kappa_3)$ is the Fourier coefficient of vorticity. Due to isotropy, the enstrophy spectrum $E^{\omega}(\kappa)$ in the inertial range can be written as

$$E^{\omega}(\kappa) = C_{\omega}\epsilon^{2/3}\kappa^{1/3}. \tag{60}$$

From an analogous relation in isotropic turbulence,

$$E_{11}^{\omega} = \int_{\kappa_1}^{\infty} \frac{E^{\omega}(\kappa)}{\kappa}\left(1 - \frac{\kappa_1^2}{\kappa^2}\right) d\kappa, \tag{61}$$

$E_{11}^{\omega}(\kappa_1)$ can be roughly estimated as follows.

$$E_{11}^{\omega}(\kappa_1) = E_{11}^{\omega}(0) - \frac{18}{5} C_{\omega}\epsilon^{2/3}\kappa_1^{1/3}\left(1 - \frac{1}{6}\left(\frac{\kappa_1}{\kappa_{max}}\right)^{5/3}\right), \tag{62}$$

where κ_{max} is the maximum wavenumber. $E_{11}^{\omega}(0) - E_{11}^{\omega}(\kappa_1)$ for the tested schemes are demonstrated in Fig. 23. The spectral scheme and CSS clearly exhibit slowly increasing behavior whereas the predictions by CS, KL1, and HT1 show a plateau and pile-up at the maximum wavenumber. Overall, the CSS produces a solution closest to the spectral solution. This confirms our claim that the wave resolving capability of a scheme near the maximum wavenumber is critical in capturing correct behavior in the inertial range as well. This suggests that when a scheme is designed, it is desirable to optimize a cost function that represents high wavenumber components equally well.

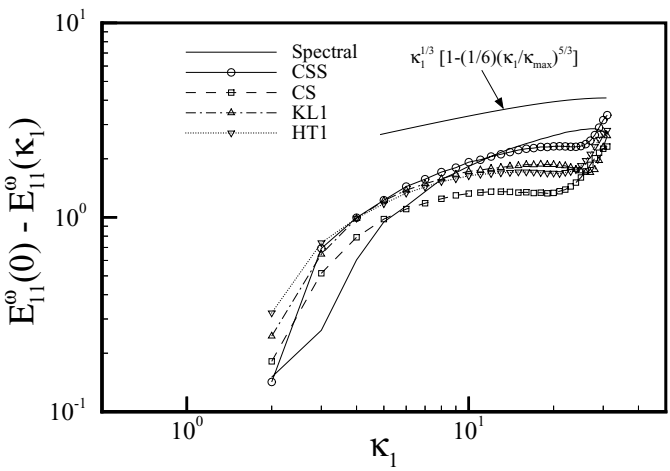

FIG. 23. One-dimensional enstrophy spectra, $E_{11}^{\omega}(\kappa_1)$, obtained by the schemes tested: solid line without symbol; solid line, CSS; dashed line, CS; chain-dotted line, KL1; dotted line, HT1.

6. CONCLUSION

Based on truncated spectral representations for the first and second derivatives, we derived a family of new compact spectral schemes with two free parameters. By imposing second- or fourth-order accuracy, these two parameters were uniquely determined. Investigation of the wave resolution property revealed that the wave resolution errors are relatively uniformly distributed in the wavenumber space compared to other optimized schemes. Through investigation of the wave resolution error and tests of the scheme in the computation of derivatives of a given function, it was shown that the wave resolution of the proposed scheme is substantially improved over the compact finite difference scheme and other known optimized schemes for the same sizes of stencils without any extra computational cost.

It may be possible to optimize a scheme the modified wavenumber of which can approximate best the exact wavenumber distribution with minimum order of accuracy maintained as was done for other optimized compact schemes. We emphasize that our scheme was derived without any optimization procedure, still being superior to any other scheme as shown in a variety of tests. This implies that an optimization in the wavenumber space does not guarantee the best performance unless the cost function to be minimized is carefully chosen to represent the real performance of the scheme. Since the function to be differentiated is not known, a priori, a choice of a particular cost function does not ensure the same performance in general applications.

The proposed scheme was tested in the numerical simulation of forced isotropic homogeneous turbulence. The proposed scheme produced an energy spectrum closest to the spectral solution among the tested schemes for the same width of stencil. It is amazing that a minor improvement in the wave resolution yields a substantial difference in the real simulation of turbulence. This is most likely due to the flat nature of the energy spectrum of turbulence. The proposed scheme is recommended for use in turbulence simulation including DNS and LES.

ACKNOWLEDGMENTS

We are grateful to the anonymous referees for very fruitful comments. We acknowledge the support by the Korea Research Foundation through Grant KRF-99-003-E00014.

REFERENCES

1. A. G. Kravchenko and P. Moin, On the effect of numerical errors in large eddy simulations of turbulent flows, *J. Comput. Phys.* **131**, 310 (1997).
2. I. Fedioun, N. Lardjane, and K. Gokalp, Revisiting numerical errors in direct and large eddy simulations of turbulence: Physical and spectral space analysis, *J. Comput. Phys.* **174**, 816 (2001), doi:10.1006/jcph.2001.6939.
3. S. K. Lele, Compact finite difference schemes with spectral-like resolution, *J. Comput. Phys.* **103**, 16 (1992).
4. P. C. Chu and C. Fan, Sixth-order difference scheme for sigma coordinate ocean models, *J. Phys. Oceanogr.* **27**, 2064 (1997).
5. K. Mahesh, A family of high order finite difference schemes with good spectral resolution, *J. Comput. Phys.* **145**, 332 (1998), doi:10.1006/jcph.1998.6022.
6. O. Holberg, Computational aspects of the choice of operator and sampling interval for numerical differentiation in large-scale simulation of wave phenomena, *Geophys. Prospect.* **35**, 629 (1987).
7. C. K. W. Tam and J. C. Webb, Dispersion-relation-preserving finite difference schemes for computational acoustics, *J. Comput. Phys.* **107**, 262 (1993).

8. P. A. Orlin, A. L. Perkins, and G. Heburn, A frequency accurate spatial derivative finite difference approximation, *Numer. Meth. Part. Diff. Eq.* **13**, 549 (1997).
9. D. P. Lockard, K. S. Brentner, and H. L. Atkins, High accuracy algorithms for computational aeroacoustics, *Amer. Inst. Aeronaut. Astronaut. J.* **33** 246 (1994).
10. N. A. Adams and K. Shariff, A high-resolution hybrid compact-ENO scheme for shock-turbulence interaction problems, *J. Comput. Phys.* **127**, 27 (1996).
11. D. W. Zingg, H. Lomax, and H. M. Jurgens, High-accuracy finite-difference schemes for linear wave propagation, *SIAM J. Sci. Comput.* **17**, 328 (1996).
12. M. Zhuang and R. F. Chen, Applications of high-order optimized upwind schemes for computational aeroacoustics, *Amer. Inst. Aeronaut. Astronaut. J.* **40**(3), 443 (2002).
13. Z. Haras and S. Ta'asan, Finite difference schemes for long-time integration, *J. Comput. Phys.* **114**, 265 (1994).
14. J. W. Kim and D. J. Lee, Optimized compact finite difference schemes with maximum resolution, *Amer. Inst. Aeronaut. Astronaut. J.* **34**(5), 887 (1996).
15. S. Gaitonde and J. S. Shang, Optimized compact-difference-based finite-volume schemes for linear wave phenomena, *J. Comput. Phys.* **138**, 617 (1997).
16. J. P. Boyd, Sum-accelerated pseudospectral methods: The Euler-accelerated sinc algorithm, *Appl. Numer. Math.* **7**, 287 (1991).
17. J. P. Boyd, A fast algorithm for Chebyshev and Fourier interpolation onto an irregular grid, *J. Comput. Phys.* **103**, 243 (1992).
18. J. P. Boyd, Sum-accelerated pseudospectral methods: Finite differences and sech-weighted differences, *Comput. Meth. Appl. Mech. Eng.* **116**, 1 (1994).
19. J. P. Boyd, *Chebyshev and Fourier Spectral Methods*, Lecture Notes in Engineering (Springer-Verlag, Berlin/New York, 1989), Vol. 49, p. 722.
20. C. Canuto, M. Y. Hussaini, A. Quarteroni, and T. A. Zang, *Spectral Methods in Fluid Dynamics* (Springer-Verlag, Berlin/New York, 1988), p. 44.
21. J. Wimp, *Sequence Transformations and Their Applications* (Academic Press, San Diego, 1981), p. 24.
22. J. Ferziger, Large eddy simulation, in *Simulation and Modeling of Turbulent Flows*, edited by T. B. Gatski, M. Y. Hussaini, and J. L. Lumley (Oxford Univ. Press, London, 1996). p. 109.
23. S. B. Pope, *Turbulent Flows* (Cambridge Univ. Press, Cambridge, UK, 2000), p. 226.